Ionization and dissociation of H_2 in intense laser fields at 1.064 μm, 532 nm, and 355 nm

A. Zavriyev,* P. H. Bucksbaum, H. G. Muller,† and D. W. Schumacher
AT&T Bell Laboratories, Murray Hill, New Jersey 07974
(Received 24 April 1990)

We present a systematic experimental study of the dissociation and ionization of molecular hydrogen in intense laser fields at three different wavelengths: 1.064 μm, 532 nm, and 355 nm. The light intensity ranges from 10^{13} W/cm^2 to 10^{15} W/cm^2. Measurements include electron spectra and angular distributions, kinetic-energy spectra and angular distributions of ion fragments, and ion dissociation fractions. We report a number of interesting and novel phenomena, including the following: above-threshold ionization to various vibrational states in the molecular ion, production of very-high-energy electrons from ionization at 1.064 μm, enhanced dissociation of the H_2^+ molecular ion via the mechanism of bond softening, above-threshold dissociation, and evidence for the alignment of the molecule in a high-intensity laser field.

I. INTRODUCTION

Recent progress in understanding atomic behavior in intense laser fields[1–4] has triggered interest in molecules in similar conditions, where the additional interatomic degrees of freedom enrich the problem. Much experimental and theoretical work has been done lately in an effort to understand better the interaction of intense light with molecules.[5–9] One of the most popular objects for study in this field is molecular hydrogen. Even though this is the simplest neutral molecule, there are still many aspects of its behavior in a light field that are not adequately understood. We present the results of a systematic experimental study of molecular hydrogen in intense light fields. Three different wavelengths were used: the Nd:YAG fundamental (where YAG denotes yttrium aluminum garnet) at 1.064 μm (ir), and its harmonics at 532 nm (green) and 355 nm (uv). The light intensity ranged from 10^{13} W/cm^2 to 10^{15} W/cm^2, providing peak electric fields of up to 10 V/Å.

Figure 1 shows a simplified potential-energy diagram for molecular hydrogen.[10] The initial state is the lowest vibrational level of the H_2 ground-state $X\,^1\Sigma_g^+$. Since the closest allowed transition is to a state 10 eV higher, all optical excitation processes involve multiple photons, and therefore require intense light. Several different multiphoton processes can contribute. For example, the molecule may be excited to a dissociative state such as $b\,^3\Sigma_u^+$ by absorption of photons, and then dissociate into two neutral atoms. The probability of this event is small because of the weak optical coupling between the singlet $X\,^1\Sigma_g^+$ ground state and the repulsive triplet state $b\,^3\Sigma_u^+$. Alternatively, the hydrogen molecule might absorb so many photons under intense irradiation that it gives up both electrons simultaneously, resulting in a final state of two bare protons. Evidence for the telltale "Coulomb explosion" following double ionization has been claimed recently in experiments involving excimer laser irradiation.[6] Finally, a less exotic third possibility is single-electron ionization, resulting in production of an H_2^+ ion in its ground state $X\,^2\Sigma_g^+ 1s\sigma_g$. The H_2^+ ion may in turn absorb more photons, leading either to dissociation or photoionization, or both. Excitation from the ion ground state into the $2p\sigma_u$ repulsive state is dipole allowed and leads to rapid dissociation into a neutral hydrogen atom and an atomic ion H^+. The fragments share the kinetic energy of dissociation almost equally, so this process can

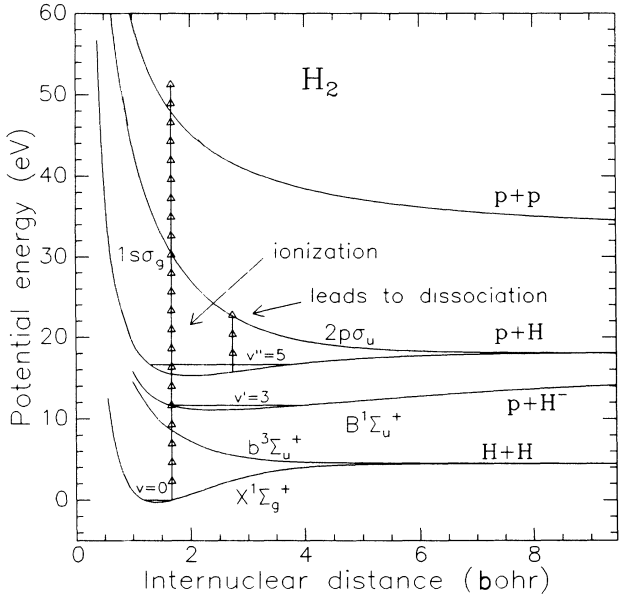

FIG. 1. Simplified potential-energy diagram for hydrogen, with the internuclear separation along the horizontal axis. The uppermost curve shows the Coulomb energy of two bare protons. Only a few relevant nuclear vibrational levels are shown: the $v=0$ vibrational level of the molecular ground state, which is the initial state of the hydrogen in this experiment; the $v'=3$ vibrational level of the B state; and the $v''=5$ vibrational level of the H_2^+ ground state. Some of the possible multiphoton processes for $\lambda=532$ nm are also shown in the figure. The vertical arrows are 2.33 eV long, and represent absorbed photons.

 ©1990 The American Physical Society

be identified easily by observing the velocities of the fragments. Among these different scenarios for decay of H_2 in an intense laser field, this last is the *main* one that we have seen in our experiments.

II. APPARATUS

These experiments use a mode-locked and Q-switched Nd:YAG laser (1.064-μm fundamental), followed by a Pockels cell, which passes a single pulse from the pulse train. The selected pulse passes through an amplifier and then a harmonic generator, which can double (532 nm) or triple (355 nm) the light frequency. The output pulse energy ranges up to 55 mJ (ir), 25 mJ for green light, and 15 mJ for uv. The pulse width ranges between 70 and 100 ps. A repetition rate of 10 Hz allows rapid collection of data.

An attenuator, consisting of a half-wave plate followed by a polarizer, controls the light intensity. An additional half-wave plate is employed to change the direction of linear polarization. A 150-mm lens focuses the light ($f/10$) to a $\approx$10-μm-diam spot inside an ultra-high vacuum chamber. Background pressure in the chamber is 1×10^{-9} Torr. During the experiments we fill the chamber with 5×10^{-8}–10^{-5} Torr of ultrapure hydrogen gas.

The vacuum chamber houses three detectors, each consisting of a pair of microchannel plates. Two detectors serve in electron and ion time-of-flight spectrometers. These spectrometers share an interaction region enclosed by mu-metal and copper cylinders, providing field-free travel for particles. The times of arrival of the particles are recorded and then converted into kinetic-energy spectra. The energy resolution of the spectrometers is better than 15 meV for 1-eV electrons and 10 meV for 1-eV protons. The channel plates subtend a small solid angle, so that by changing the angle of the light polarization we can observe the angular dependence of the signal in the azimuthal plane (perpendicular to the direction of the light propagation). The acceptance angle of the electron detector is $\approx10^{-4}$ sr and that of the ion detector is $\approx10^{-3}$ sr. The third detector views a separate interaction region in which a static electric field of up to 1000 V/cm sweeps all the positive ion into the plates. Time-of-flight data obtained in this way provide information about the charge-to-mass ratio of the fragments, enabling measurements of the relative abundance of H_2^+ and H^+ following the laser interaction.

Despite the presence of the electrostatic and magnetic shield, we have found that small static fields due to charge buildup on surfaces, or patch effects, can affect the time-of-flight spectra. Therefore independent calibration methods are necessary. We use very-well-known xenon photoelectron spectra to calibrate the electron spectrometer.[3,11] The ion spectrometer is more difficult to calibrate, and several different methods are used. Its length can be measured directly. In addition, spectra from foci with different flight path lengths may be compared. An independent test of the calibration can be obtained from the charge-to-mass ratio spectrometer: ions emitted back-to-back along the extraction field lines reach the detector at different times, determined by their dissociation kinetic energy.[7] Unfortunately, none of these calibrations are as accurate as the calibration of the electron spectrometer; we assign a systematic error of 15% to our ion kinetic-energy spectra.

The gas density is kept very low in order to minimize the effects of space charge due to the positive ions left behind when the electrons move out of the focus. Space charge tends to lower and broaden the features in electron kinetic-energy spectra. Ion spectra, on the other hand, tend to broaden to higher energy.

III. DATA

A. 532 nm

1. *Electron spectra and total ion yield versus intensity*

The characteristic feature of all above-threshold ionization (ATI) photoelectron spectra is the presence of peaks separated by the photon energy (2.33 eV). In H_2 irradiated by 532-nm light, not one but several series of ATI peaks appear, whose relative positions and magnitudes depend on the light intensity and polarization. The lower distribution shown in Fig. 2 (marked by symbol A)

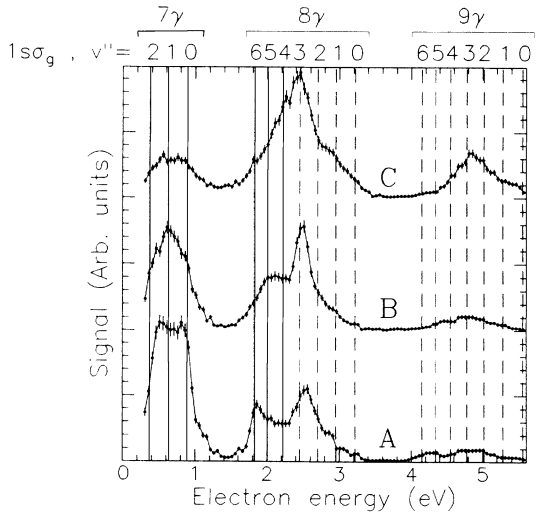

FIG. 2. Dependence of the 532-nm electron kinetic-energy spectra on light intensity. The lowest graph (marked A on the figure) shows a distribution of approximately 9000 electrons collected during 5000 laser shots at a peak light intensity of 5×10^{13} W/cm^2. The density of hydrogen was 3.5×10^{11} cm^{-3}. The other two traces are spectra at peak intensities 7×10^{13} W/cm^2 (B) and 1×10^{14} W/cm^2 (C). The densities during these runs were reduced to (3.5×10^{10} cm^{-3} and 5.3×10^{10} cm^{-3}), respectively. Error bars are statistical. Vertical lines indicate expected electron energies for ionization into different vibrational levels of the H_2^+ ground state (the values of v'' are marked on top of the figure). Solid lines indicate threshold ionization peaks, i.e., those with the minimum possible number of photons. Dashed lines show the expected positions of ATI peaks. These peaks are clustered by the total number of photons absorbed (marked on top of the figure).

is typical of what we call "the low light-intensity regime." It is obtained by collecting the photoelectrons during 10^4 laser shots with a peak light intensity in the center of the focus equal to 5×10^{13} W/cm^2. Here and after we calculate peak intensity assuming a Gaussian focal profile. In the runs shown in Fig. 2 the electrons are detected along the laser polarization.

When the light intensity is increased (7×10^{13} W/cm^2 for regime *B* at the graph and 1×10^{14} W/cm^2 for curve *C*) the electron energy spectrum changes. The different series of peaks seem to merge into one series of broad and fairly featureless peaks extending to higher energy than before.

An additional piece of information helps to explain this rather dramatic intensity effect. Figure 3 shows the dependence of the total yield of H_2^+ and H^+ versus the laser peak intensity. The "low-intensity" photoelectron spectrum in Fig. 2 was obtained at the intensity labeled *A*, while the other two spectra match intensities at points *B* and *C*. Figure 3 shows that in the low-intensity regime, 90% of the residual ions are H_2^+. Hence most of the electron signal comes from the photoionization of the hydrogen molecule H_2 to produce the molecular ion. The positions of the peaks in this spectrum corroborate this hypothesis: they correspond to above-threshold ionization from the hydrogen ground state to the different vibrational levels of the ionic ground state. The peak positions should be given by

$$E_i = n\hbar\omega - E_{\rm ion}^{v''}(I) + E_{\rm mol}^{v=0}(I) + U_P \ , \tag{1}$$

where $E_{\rm ion}^{v''}(I)$ is the ion's energy in the v''th vibrational level of the ground state $1s\sigma_g$, and $E_{\rm mol}^{v=0}(I)$ is the energy of the $v=0$ molecular ground state, both evaluated at light intensity I. If the shift in ionization potential is equal to the ponderomotive shift U_P, as anticipated from the results of ATI experiments on atoms,[3,4] then for the duration of the pulses used, we expect peaks at

$$E_i = n\hbar\omega - E_{\rm ion}^{v''}(0) + E_{\rm mol}^{v=0}(0) \ , \tag{2}$$

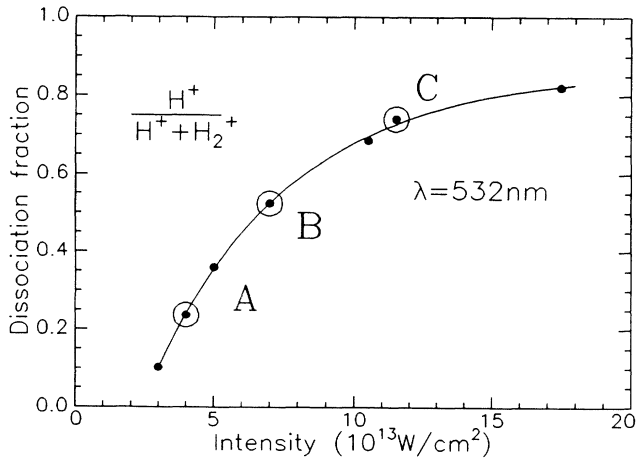

FIG. 3. Dissociation fraction of H^+ ions as a function of laser intensity for 532-nm light. *A*, *B*, and *C* mark the positions for the spectra shown on Figs. 2(a) and 2(b).

where all the energies are given at zero intensity. These positions for $n=n_{\rm min}$ are indicated by solid vertical lines on Fig. 2 ($n_{\rm min}$ is the minimum number of photons required to ionize the H_2 molecule in the $v=0$ vibrational level of the ground state into v''th vibrational level of the H_2^+ ground state). It is important to note that $n_{\rm min}$ depends on v''. The vertical dashed lines on Fig. 2 mark the expected positions of the ATI peaks for different vibrational levels of the molecular ion, assuming there is no change in the rotational state.

The peaks in the spectra in Fig. 2 appear grouped together according to the number of photons absorbed by the molecule during ionization. Almost half of the detected photoelectrons have energies below 1.3 eV (these electrons come from the seven-photon ionization of H_2). About 40% of the electrons come from the eight-photon ionization of molecular hydrogen (the kinetic energy of these electrons ranges between 1.3 and 3.5 eV). The rest of the photoelectrons come from molecules that have absorbed nine or more photons (energies above 3.6 eV).

During the highest-intensity run (*C* in Figs. 2 and 3) 90% of the H_2^+ molecular ions dissociate into hydrogen atoms and protons (H^+). Neutral hydrogen atoms may in turn photoionize, producing electrons with energies given by

$$\begin{aligned} E_i &= n\hbar\omega - \mathcal{E}_{\rm H} - U_S^{\rm g.s.} \\ &= 0.38\ {\rm eV} - U_S^{\rm g.s.},\ 2.71\ {\rm eV} - U_S^{\rm g.s.}, \ldots , \end{aligned} \tag{3}$$

where $U_S^{\rm g.s.}$ and $\mathcal{E}_{\rm H}$ are, respectively, the ac Stark shift of the ground state and the ionization potential of atomic hydrogen. We assume here that the shift of the atomic ionization potential is equal to the ponderomotive potential. In each of the rare gases and other cases that have been studied in ATI, the Stark shift of the ground state of the atom is nearly equal to the shift of the ground state of the ion.[3] In that case, there is almost no contribution to the photoelectron energy from the ground-state shift. However, this cancellation does not happen for atomic hydrogen, where the final-state ion is a bare proton. The ac Stark shift of the ground state of atomic hydrogen can be estimated by the dc Stark shift, or the product of the dc polarizability and the light intensity.[8] For our intensity range it is approximately 400 meV in the most intense parts of the pulse. In the less intense parts of the pulse (spatial and temporal) the ac Stark shift should be even less. This spectral shift must be averaged over the parts of the laser focus where the ionization occurs, to calculate the photoelectron spectrum. Trace *C* in Fig. 2 shows peaks corresponding to a ground-state atomic ac Stark shift of $\approx$200 meV, which is consistent with this estimate and supports the hypothesis that dissociation produces atoms in the ground state.

Another feature of the high-intensity photoelectron spectrum is the relative reduction of the low-energy peaks. There are two effects that contribute to this. The first is so-called "channel cutoff."[4] As the pondermotive potential goes up with the light intensity, so does the ionization potential. At the moment when the shift in ionization potential exceeds $\hbar\omega$, the minimum number of photons required for ionization increases by 1, suppress-

ing the lowest-energy peak. The second contribution to reduction of signal in the low-energy ATI peak is the scattering power of the ponderomotive force. Electrons tend to be emitted along the laser polarization, so the signal is strongest when the polarization is aligned with the spectrometer. Ponderomotive forces will divert the electrons along the negative gradients of the laser intensity, producing a more isotropic distribution.[2] This effect is most pronounced for the lowest-energy electrons.

2. *Proton energy spectra*

Figures 4 and 5 show typical proton kinetic-energy spectra for 532-nm light. Most of the detected protons (90%) are concentrated in one broad peak around 0.4 eV. The proton spectrum also features higher-energy peaks separated by $\hbar\omega/2$. As the laser intensity increases the low-energy peak broadens to lower energies.

Figure 5 also displays the angular distributions of H^+ fragments emitted in a plane perpendicular to the direction of light propagation. Each distribution features protons in an energy range within 20 meV of one of the peaks in the proton energy spectrum, as shown by the arrows. At the lower intensity (5×10^{13} W/cm^2 at the peak) the distribution is narrowly peaked around the polarization direction. Evidently, most of the ions dissociate along the light polarization. It seems clear that the direction of the fragments must be nearly aligned with the internuclear axis, since that is the direction of the dissociative potential gradient, and the low-intensity laser field cannot change it very much. Thus we conclude that most molecules that dissociate are aligned with the field. This is not surprising; there is an enhanced dipole coupling between the H_2^+ ground state and the $2p\sigma$ dissociative state for molecules aligned with the laser polarization[9] because these two states are just the symmetric and antisymmetric combinations of an electron nearby two protons.

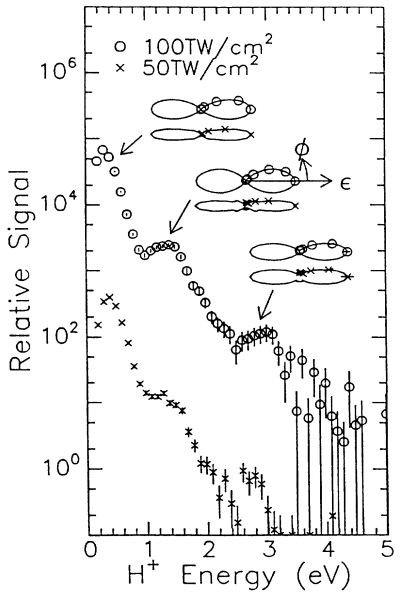

FIG. 5. Energy spectrum and angular distribution of ions dissociated during photoionization of H_2 by 532-nm linearly polarized light. The spectra shown here are the same as the ones on Fig. 3(a). Above 5×10^{13} W/cm^2 the proton spectra develop a series of peaks separated by $\hbar\omega/2=1.165$ eV. Protons are emitted along the laser polarization $\bar{\epsilon}$ in narrow distributions that become broader as the intensity increases.

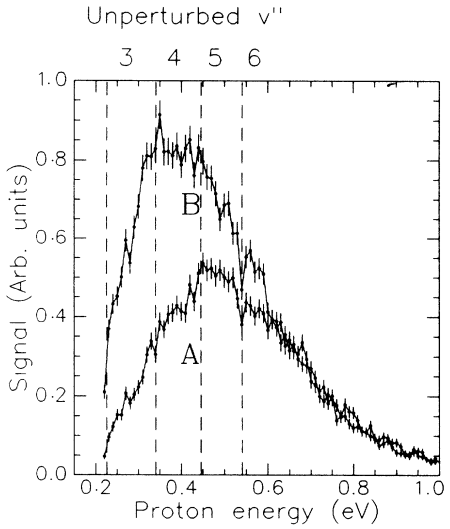

FIG. 4. Intensity dependence of proton spectra for 532-nm light. The lower spectrum was collected at a light intensity of 5×10^{13} W/cm^2, and a density of 3.5×10^{11} cm^{-3}. For the upper curve, the intensity was doubled (10^{14} W/cm^2) and the gas density lowered to 3.5×10^9 cm^{-3} in order to avoid space-charge effects. Each run detected approximately 1.5×10^4 protons over 10^4 laser shots. The light was linearly polarized, and the protons were collected along the direction of polarization. The expected proton energies for different unperturbed vibrational levels of the H_2^+ ground state are marked along the bottom of the figure. As the light intensity increases, the relative amount of slow protons coming from dissociation of the ions in the lower vibrational levels increases.

When the laser intensity is doubled (1×10^{14} W/cm^2), Fig. 3 shows that nearly all of the molecules dissociate. However, the angular distributions in Fig. 5 are still strongly aligned with the laser field, although they are somewhat broader. Evidently, something has happened to force the molecules to align and dissociate. In fact, we will show below that the laser field does begin to exert a significant torque on the molecule, leading to alignment followed by dissociation, and to the specific form of the proton spectrum shown in Fig. 5. These are manifestations of a new high-field effect that we call "bond softening," which will be explained below.

B. Ultraviolet data

1. *Electrons*

A typical 355-nm photoelectron spectrum is shown in Fig. 6. Like the 532-nm photoelectron distribution, the uv spectrum also features several ATI peaks, with fine structure associated with the vibrational levels of the

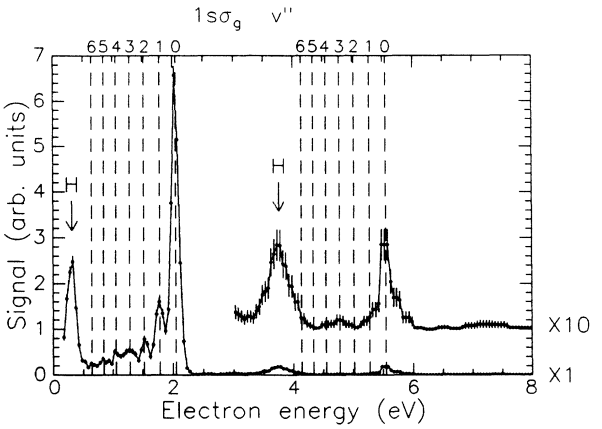

FIG. 6. Photoelectron energy spectrum of H_2 at 355 nm, for electrons emitted in the direction of the polarization. Peak intensity at the focus: 1×10^{14} W/cm^2; density: 1.8×10^9 cm^{-3}. Most of the signal is due to ionization into different vibrational levels of the H_2^+ ground state. The remainder is from ionization of atomic hydrogen (as shown by arrows).

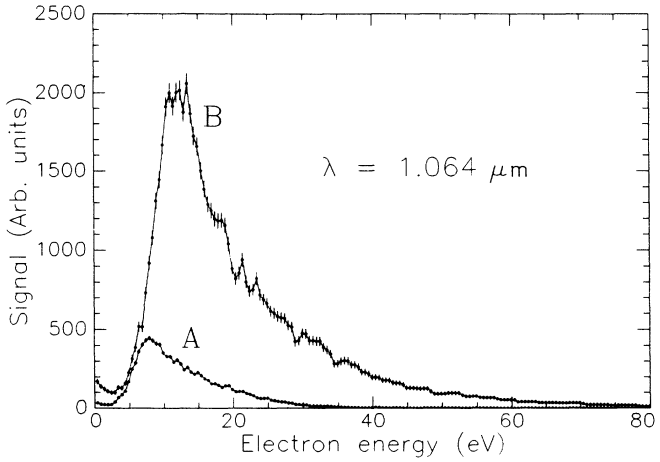

FIG. 8. Dependence of the 1.064-μm photoelectron energy spectra on light intensity. Lower curve (2.2×10^{14} W/cm^2): 2×10^4 electrons, collected over 10^4 laser shots; density: 1.1×10^{10} cm^{-3}. Upper curve (1.1×10^{15} W/cm^2): 3.3×10^4 electrons, collected over 10^4 laser shots; density: 1.2×10^9 cm^{-3}.

ground state of H_2^+. Most of the electrons (about 90%) are in the threshold peaks. The remaining 10% mimic the lower-energy distribution, at a higher-energy separated by one photon (3.495 eV). Most of the signal is due to transitions from the ground state $X\,^1\Sigma_g^+(v=0)$ to various vibrational levels v'' of the H_2^+ ground state, just as for 532-nm radiation in the low-intensity regime. The rest of the signal ($\approx$25%) comes from the ionization of atomic hydrogen. Within the available intensity range, we did not see any dependence of the shape of this uv photoelectron spectrum on intensity.

2. *Protons*

The presence of electrons from the photoionization of atomic hydrogen in Fig. 6 indicates some dissociation during the laser pulse. Confirmation of this comes from direct measurements of the proton kinetic-energy spectrum for 355-mn light, shown in Fig. 7. The extreme low-energy peak that dominated the proton spectrum at 532 nm is not present in the uv data. Instead, the protons appear in a broad peak ($\Gamma=0.7$ eV) centered at 0.8 eV. Other researchers have observed a component of very fast (>12 eV) protons coming from dissociation of H_2 with 308-nm light at much lower peak intensity.[6] Runs with different (lower) light intensity were performed to

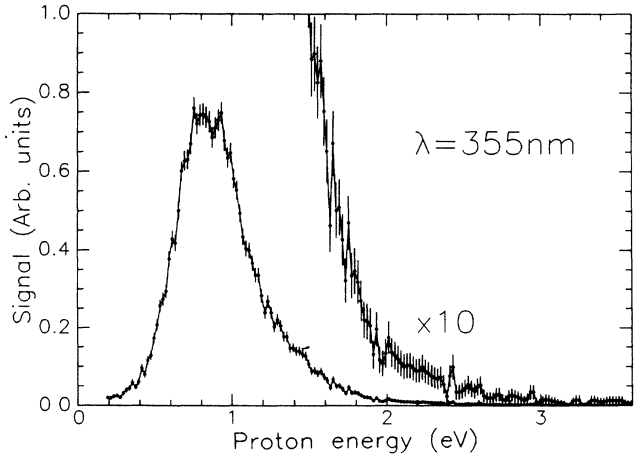

FIG. 7. Typical proton kinetic-energy spectrum for linearly polarized 355-nm light. The protons were detected along the polarization. The protons are grouped in a broad peak (full width at half-maximum is 0.7 eV) around 0.8 eV. Light intensity: 1×10^{14} W/cm^2, density: 1.8×10^{10} cm^{-3}.

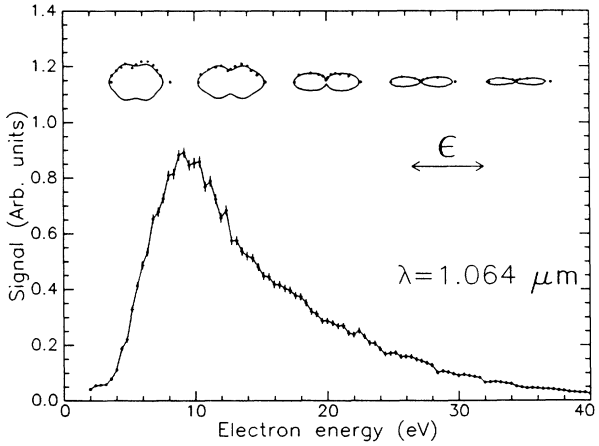

FIG. 9. Energy spectrum and angular distribution of electrons emitted during photoionization of H_2 by linearly polarized 1.064-μm light. The laser polarization was rotated in 15-deg increments from 0° to 180°. Each run contains 2×10^4 laser shots. Peak intensity: 8×10^{14} W/cm^2; density: 3.5×10^9 cm^{-3}. The figure shows the spectrum for electrons emerging in the polarization direction. The angular distributions become narrower with kinetic energy, implying that most of the electron energy does *not* come from ponderomotive scattering.

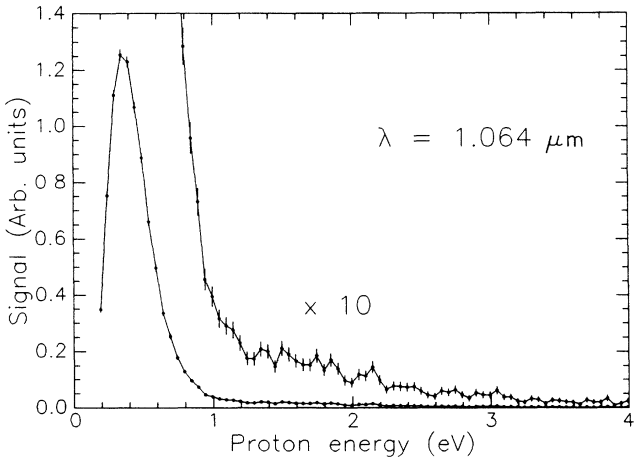

FIG. 10. Proton kinetic-energy spectrum, containing $\approx 2.9\times10^4$ protons, collected during 2×10^4 laser shots. Peak intensity: 5×10^{14} W/cm^2; density: 7×10^{10} cm^{-3}. Most of the dissociating protons collected during photoionization of H_2 by 1.064-μm light are grouped in a low-energy peak around 0.35 eV. The rest are in the peaks separated by $\hbar\omega/2=0.58$ eV as seen from the enlargement shown.

look for this effect at 355 nm; however, no significant intensity-dependent effects were observed.

C. Infrared data

1. Electrons

Infrared photoelectron spectra in H_2 (Figures 8 and 9) differ from any other ATI results we have seen, in that there are no distinct ATI peaks: The electrons appear in a single very broad asymmetrical distribution. A typical ir photoelectron spectrum shows very few electrons with kinetic energies lower than 5 eV. The electron distribution increases from around 5 eV to a peak varying between 10 and 15 eV, depending on the light intensity. At still higher electron energies, the signal decreases slowly. In most ATI experiments using Nd:YAG light or its harmonics, electron energies do not exceed 20 eV; in the case of H_2, however, we have observed electrons with energies up to 100 eV.

Both the peak and the high-energy tail of the 1.064-μm H_2 photoionization spectrum increase with intensity. Figure 8 shows the ir photoelectron energy spectra for two different values of the peak laser intensity. The limit of the high-energy tail increases approximately linearly with intensity, and its end-point value is in the range of the peak pondermotive potential in the laser pulse. High statistics were collected in order to explore possible substructure in the relatively featureless ir photoelectron spectrum. We concluded that, with the exception of slight modulations at the photon energy, none of the structure in ir electron energy spectrum is statistically significant.

Figure 9 also shows angular distributions of electron signal in the azimuthal plane for different electron kinetic energies. The angular distributions are centered over the corresponding energies. The peaks in the distribution lie along the laser polarization vector. The anisotropy of these distributions can be used to estimate the value of the ponderomotive potential in the part of the focus where most of the photoionization took place. This will be analyzed further below.

2. Protons

A typical ir proton spectrum is shown in Fig. 10. Most of the signal ($\approx$93%) is grouped in a broad ($\Gamma=0.6$ eV) peak around 0.35 eV. The remainder is in the high-energy shoulder, which is not as prominent as the higher-energy features for 532-nm light. There was no observable intensity dependence in the shape of this spectrum.

IV. DATA ANALYSIS (uv AND GREEN)

As described above, the electron spectra at 532 nm display two laser-intensity regimes. Initially the intensity is too low to provide an appreciable photoionization signal. Above $(3-5)\times10^{13}$ W/cm^2, photoelectrons appear in clusters of peaks. This is the *low-intensity regime.* Spectra at 355 nm display similar behavior. Above $\approx1\times10^{14}$ W/cm^2, the 532-nm photoelectron spectrum changes to a series of broad peaks separated by $\hbar\omega$ called the *high-intensity regime.* This regime was not observed for 355-nm light.

In both uv- and green-induced electron spectra, most of the peaks appear at energies identified with multiphoton ionization from the H_2 ground state to different vibrational levels of the H_2^+ ground state. Different paths are available for this process. First, the molecule might make a direct transition from the zeroth vibrational level of the $X\,^1\Sigma_g^+$ ground state into the molecular ion $X\,^2\Sigma_g^+ 1s\sigma_g$ ground state. This would require at least seven photons at 532 nm—eight photons for the higher vibrational levels of the H_2^+ ground-state manifold.

An alternative lower-order pathway to the molecular ion involves a direct transition to an intermediate excited state of H_2. For example, a good candidate for excitation at 532 nm is the B state ($^1\Sigma_u^+ 2p\sigma_u$), which has low-lying vibrational levels near the five-photon resonance for 532-nm light. In a recent experimental paper, Verschuur, Noordam, and van Linden van den Heuvell have proposed that the $B\,^1\Sigma_u^+(v'=3)$ five-photon resonance and $GK\,^1\Sigma_g^+(v'=2)$ six-photon resonance may contribute most of the ionization signal.[8] These two states are almost at resonance *if ac Stark shifts are neglected.* However, we would expect these resonance conditions to have a strong intensity dependence, similar to that observed in sub-picosecond ATI experiments in atoms.[12] Even without performing detailed calculations, we can make a few general statements about the magnitude of these shifts. The ponderomotive potential U_P sets the energy scale for ac Stark shifts between the tightly bound ground state and more weakly bound excited states. Therefore, at laser intensities where photoionization is observed,

where U_P is above 0.2 eV, these states should shift out of resonance. Other lower-lying vibrational levels may come into resonance as well.

For 355-nm light the $B\ ^1\Sigma_u^+$ state is not near resonance. However, the $GK\ ^1\Sigma_g^+(v'=2)$ state is near a four-photon resonance with the molecular ground state. The ponderomotive potential is reduced by over a factor of 2 from 532-nm light at the same intensity. In addition, the intensities where ATI is seen are lower. Therefore Stark shifts will be less important at 355 nm.

The transition probability between two vibrational levels is proportional to the square of the overlap of the two corresponding wave functions, the so-called Franck-Condon factor (FCF).[13] The FCF's for ionization of the B state ($v'=0,1,2,3$) into different vibrational levels of the ionic X state are shown in bargraphs in Fig. 11 (they are calculated for both states unperturbed). The Franck-Condon factors for transitions between $GK(v'=2)$ and the vibrational states of H_2^+ have been published previously.[8] The data show poor agreement between individual electron peaks and the corresponding FCF's. There may be several factors contributing to the disagreement. First, since the internuclear potential energy curves of the H_2^+ ground state change with intensity (see below), the Franck-Condon factors also change. This may cause

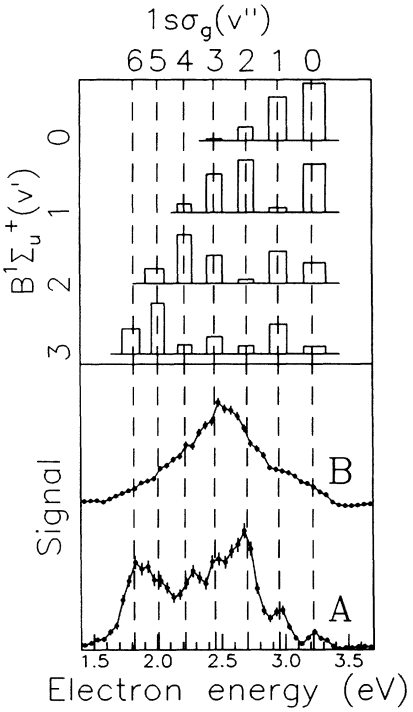

FIG. 11. This figure displays the Franck-Condon factors for photoionization into different vibrational states of H_2^+, assuming that the process is resonantly enhanced by five-photon excitation into different vibrational levels (v') of the $B\ ^1\Sigma_u^+$ state. The ac Stark effect shifts lower vibrational levels of $B\ ^1\Sigma_u^+$ into resonance at higher light intensity. Eight-photon photoelectron spectra A and B are shown for comparison. Light intensities during these runs were the same as those for A and C on Fig. 2(a).

hydrogen to photoionize to different vibrational levels of H_2^+, depending on the light intensity at the moment of ionization.

In addition, the energies of the excited states of H_2 shift in and out of resonance with intensity. For example, in photoionization by 532-nm light, the third vibrational level of the $B\ ^1\Sigma_u^+$ state is in five-photon resonance with the ground state at low intensity. As the light intensity increases, the $B\ ^1\Sigma_u^+$ state is expected to shift up, so that the second, first, and finally zeroth vibrational levels of $B\ ^1\Sigma_u^+$ state come into five-photon resonance. Assuming that most of the shift comes from the ponderomotive energy of electrons, we calculate that these levels become resonant at the following intensities: $v'=2$ at 5.5×10^{12} W/cm^2, $v'=1$ at 1.1×10^{13} W/cm^2, and $v'=0$ at 2×10^{13} W/cm^2. Since the excitation process to the B state is highly nonlinear, the transition probability might be enhanced at the lower vibrational levels, even if FCF's favor transitions to higher levels.

At 532 nm the sixth photon, 14 eV above the ground state, is near resonance with a gerade state GK whose $v'=0,1$ levels lie between 13.5 and 14 eV. Although this state has a double minimum, FCF considerations favor transitions into the deeper potential well. This has nearly the same shape as the H_2^+ ground state, so that a $\delta v=0$ propensity rule holds.

The shift of either the B or GK resonances to lower vibrational quantum number at higher intensity increases the transition rate for transitions to lower vibrational levels of the H_2^+ ground state at higher light intensity. On the other hand, the Franck-Condon overlap between the *molecular* hydrogen ground state and the vibrational levels of B or GK decreases for lower v': for example, the FCF for the transition from $X(v=0)$ to $B(v'=3)$ is 4.55×10^{-2}; to $B(v'=2)$ is 2.91×10^{-2}; to $B(v'=1)$ is 1.42×10^{-2}; and to $B(v'=0)$ is 0.4×10^{-2}. Competition between these two effects may influence the shape of the photoelectron spectrum.

For excitation by 355-nm light, the B state plays no role; but the GK state is near an allowed four-photon resonance. Here we see some clear evidence for enhancement of the ionization due to intermediate transitions to a lower vibrational level of GK, shifted into resonance by the ac Stark shift. The predominant final state as determined by the electron spectrum is a peak at 2.05 eV. The GK resonance at $v'=2$ (unshifted) does not have FCF's favoring this transition. However, assuming that an ac Stark shift approximately equal to the ponderomotive potential is present, we find that $v'=2$ is not the state in resonance. Rather $v'=1$ comes into resonance at $I=2\times10^{12}$ W/cm^2, followed by $v'=0$ at an intensity of 4.3×10^{12} W/cm^2. Following the arguments of the preceding paragraphs, we expect the strongest transitions for the highest intensity resonance. Then, following the $\delta v=0$ propensity rule described above, we predict that ionization into $v=0$ final state of H_2^+ should dominate, producing 2.05-eV photoelectrons, as seen.

The uv electron spectra presented here have been seen previously by Verschuur, Noordam, and van Linden van den Heuvell, who proposed an entirely different explanation based on doubly excited states.[8] Neglecting ac Stark

shifts, they suggested that illumination at 355 nm leads to direct excitation to the $GK(v'=2)$ state. This state lies near the local potential maximum in the double-well GK potential, and mixes with a dissociative doubly excited state. This then leads to the production of copious amounts of atomic hydrogen in the $n=3$ state. At the intensities needed for the multiphoton excitation of GK, the $H(n=3)$ ionizes rapidly. The resulting photoelectrons have energies which nearly match those seen in our two spectra, which we believe come from the formation of $H_2^+(v=0)$.

These two possible explanations of the origins of the uv spectra seen in our two experiments can be resolved with some additional information: the kinetic-energy spectrum of the fragments of the dissociation. The mechanism suggested by Verschuur, Noordam, and van Linden van den Heuvell must produce a peak in the proton energy distribution around 0.5 eV. Figure 7 shows that there is no increase in the proton signal around 0.5 eV, so that we have to conclude that ionization of excited atomic hydrogen is not a dominant process in our conditions.

To summarize this section, we find that under illumination at 532 and 355 nm, the dominant absorption process is the ionization of molecular hydrogen into different vibrational levels of the ground-state molecular ion H_2^+. This is followed by a strong intensity-dependent dissociation at 532 nm. There is no evidence for any form of dissociation which precedes the initial ionization of the molecule.

V. PROTONS, BOND SOFTENING, AND ABOVE-THRESHOLD DISSOCIATION

A. 532 nm

As we have shown in Sec. IV, the ultimate dissociation of the hydrogen molecule in intense 532-nm light always begins with single ionization and the formation of the H_2^+ molecular ion. This subsequently dissociates with increasing probability at higher intensities into fragments with the spectra and angular distributions displayed in Fig. 5. How does this dissociation occur?

A key to understanding the 532-nm proton spectra is the observation that the fragments tend to separate in the direction of the laser polarization (see Fig. 5). This naturally suggests dissociation via transitions to the repulsive $2p\sigma_u$ state shown in Fig. 1, since dipole transitions from the ground state to this state are maximum for molecules oriented along the laser polarization. However, there are two puzzling features that both suggest that some new high-field phenomenon is occurring: first, the molecular fragments tend to emerge along the laser polarization, even when the dissociation *fraction*, i.e., the fraction of molecular ions that dissociate, tends toward unity. It seems that the randomly oriented molecules are being aligned by the field. The second and still more puzzling problem is the energy distribution of the emerging fragments. The proton spectrum peaks at about 0.4 eV, and since each fragment carries approximately a half of the total energy released in dissociation, this means that the transition between the H_2^+ ground state and the $2p\sigma_u$ state must have occurred at an internuclear separation of $R \geq 2.5$ Å. However, most of the populated vibrational levels of H_2^+ are confined to much smaller distances. Thus it seems that this dissociation mechanism is forbidden by energy conservation at the internuclear distance of the occupied states. If this mechanism can proceed, the potential must be severely distorted by the field.

We have calculated the distortion of the ground state $1s\sigma_g$ and repulsive state $2p\sigma_u$ in the presence of a strong laser field at 532 nm. We find that the existence of a strong dipole coupling between these states does indeed lead to dramatic distortion and ultimately to dissociation of nearly all of the vibrational states. We call this new high-field process "bond softening," because the bond distortions can be thought of as a reduction in the screening of the nuclear Coulomb repulsion by the binding electron. The bond softening mechanism was also recently proposed by Guisti-Suzor *et al.*, who reached similar conclusions.[9]

To calculate the H_2^+ molecular potentials in the presence of a strong laser focus, we treat the laser field as a periodic perturbation to the molecular Hamiltonian. The Hamiltonian may then be divided into three parts: molecule, field, and interaction:

$$H = H_{\text{mol}} + H_{\text{field}} + e\mathbf{r}\cdot\mathbf{E}(t) \ . \tag{4}$$

Schrödinger's equation may be solved using Floquet methods to find the electronic eigenvalues as a function of the field strength.[14] We performed Floquet analysis for both uv and green light, for different intensities, and internuclear separations. The calculations are outlined below.

Prolate spheroidal coordinates are most convenient for H_2^+. They are

$$\xi \equiv \frac{R_A + R_B}{R}, \quad \zeta \equiv \frac{R_A - R_B}{R} \ , \tag{5}$$

where R_A and R_B are the distances between the electron and two nuclei A and B, and R, is the internuclear distance. We used electronic basis states of the form

$$\chi_i = \xi^{N_i} \zeta^{M_i} e^{-\alpha_i \xi} \ , \tag{6}$$

where N_i and M_i are integers, α_i is real, and $\alpha_i > 0$. The third coordinate, the azimuthal angle, is not important since the wave functions do not depend on it. In order to obtain the desired accuracy, three even and four odd basis states were needed, where the state is odd or even if M_i is odd or even.

The Floquet calculation is straightforward and, in fact, is essentially similar to a somewhat more sophisticated treatment that has just been published.[9] The basic idea involves dressing the bare molecular states by the laser field. Each state is taken to be the product of a wave function of the molecular variables times a discrete photon number state $|n\rangle$ with n photons. (The actual value of n in our experiment is huge, but that does not matter in the calculation; n only appears expressed as a field strength, and need not be calculated explicitly.) Our calculation used ten "Floquet blocks," where each block refers to a set of the seven basis states with one photon

state, $|n-4\rangle$ through $|n+5\rangle$. Using this basis, the Hamiltonian matrix $H_{ij}=\langle\psi_i|H|\psi_j\rangle$ consists of two different kinds of nonzero elements: elements in the diagonal blocks where $n_i=n_j$ and off-diagonal blocks where the interaction Hamiltonian couples states with $\Delta n=\pm 1$ and different parity. This simplifies the diagonalization, allowing us to treat only half of the matrix. Finally, when the entire matrix is diagonalized, the result is a series of "quasieigenvalues" of molecular states in the field. Although the basis allows for seven wave functions per Floquet block, we only concerned ourselves with the eigenvalues representing the ground states $1s\sigma_g$ and $2p\sigma_u$. These two states are only coupled by the component of the laser field polarized along the line connecting the nuclei.

Since the Floquet matrix was finite, and in fact relatively small, there were significant "edge effects," i.e., perturbations in the quasieigenvalues at the edges of the matrix due to the absence of more Floquet states above or below. To minimize these effects, we only used the quasieigenvalues in the central Floquet blocks; however, the finite number of blocks limits the reliability of the calculation somewhat.

The results of this *ab initio* calculation for 532-nm light are shown in Fig. 12. The quasieigenvalues corresponding to the two states in question are plotted versus internuclear distance to trace out the ground-state and repulsive-state potentials. Curves are plotted for several different "parallel intensities" $I_{\rm pl}$, i.e., intensities of the polarization *component* along the internuclear axis.

$$I_{\rm pl}=I_{\rm tot}(\cos\theta)^2 \ . \tag{7}$$

As $I_{\rm pl}$ increases, the $1s\sigma_g$-$2p\sigma_u$ coupling deforms the potential at points where two curves are separated by $1,3,5,\ldots$ photons. These points correspond to allowed resonant multiphoton transitions between the states. In the Floquet picture these are crossings, where eigenvalues of states in different blocks are degenerate. The dipole interactions lead to the opening of gaps, or avoided crossings, between the states at these points. As the $1s\sigma_g$ potential curve shifts adiabatically onto the $2p\sigma_u$ curve, or vice versa, the number of photons changes accordingly. These "adiabatic" transitions correspond to the excitation of the H_2^+ ion from $1s\sigma_g$ state into the repulsive $2p\sigma_u$ state by absorption and stimulated emission of many photons, resulting in the net absorption of $1,3,5,\ldots$ additional photons. The opposite process can also take place, where an ion in a repulsive state moves to the ground state by emission of an odd net number of photons. Crossings involving even numbers of photons are forbidden by parity conservation, so that curves do cross at those points.

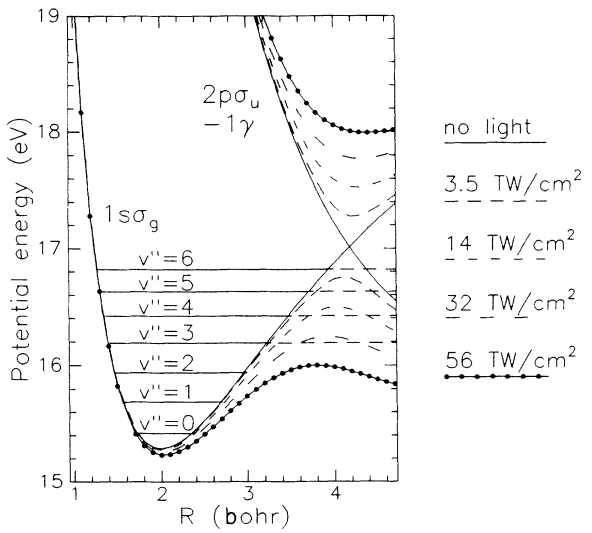

FIG. 12. One-photon crossing for 532-nm light. Solid lines show the potential curve of the unperturbed $1s\sigma_g$ state and the $2p\sigma_u$ state lowered by $\hbar\omega$. The component of the laser field parallel to the internuclear axis perturbs the states onto new curves. As the parallel polarization grows, the gap between the states opens, the binding energy of the H_2^+ ion decreases, and more vibrational states become unbound.

The gaps opened up between states by the dipole interactions with the laser field can lead to severe deformations of the internuclear potential (see Fig. 12). In the weak-field limit, any vibrational states whose eigenvalue lies above the one-photon crossing point would be unstable, since one-photon transitions to the dissociative state are allowed. However, once the avoided crossing gap opens up, lower states that lie below the middle of the gap, but above the bottom of the gap, must become unstable as well. As the parallel light intensity increases, the curves move farther and farther away from their unperturbed positions. Ultimately, the gap even drops below the lower lying vibrational levels of the H_2^+ ground state that are populated by ATI of H_2, thereby allowing them to dissociate at the one-photon crossing. This is the effect that we call *bond softening*.

A small amount of dissociation may occur, even if the vibrational state is below the bottom of the one-photon crossing gap, due to quantum-mechanical tunneling. This effect is considered by Giusti-Suzor *et al.* in their recent paper.[9] We have neglected this contribution to dissociation in our calculations.

The higher-order crossings also form gaps, representing multiphoton transitions. The molecular fragments from these events emerge faster since more photons are absorbed. The competition between these multiphoton transitions and the single-photon dissociations leads to a spectrum with several kinetic-energy peaks, shown in Fig. 5. The peak ratios depend on molecular orientation, laser intensity, and the time history of the laser pulse. For example, consider an ion created by multiphoton ionization of H_2 near the beginning of a laser pulse, where the parallel intensity is low so that the potential curves are not perturbed from their diabatic shapes. Following ionization the ion is subjected to increasing intensity. In addition, it may be rotating into alignment with the field, thereby increasing its *parallel* intensity. We would like to calculate the probability that the molecule will evolve along a given trajectory in the potential diagram. At each intersection in the diagram there is a possibility of avoiding the crossing by making an adiabatic transition to a different curve or jumping over the crossing by fol-

lowing the diabatic path. To calculate these probabilities, we employ a simple Landau-Zener theory.

The basic idea may be stated in semiclassical terms, where we imagine that the molecule is a particle moving in the internuclear coordinate along the potential shown in Fig. 12. As the molecule moves through the crossing point, it will follow the adiabatic curve so long as its rate of passage through the gap is slow compared to the Rabi rate $V_{12}/\hbar$ for transitions between the interacting states.[15] The Rabi rate is related to the size of the gap Δ:

$$\Delta = 2|V_{12}| \ . \tag{8}$$

The Landau-Zener formula yields probabilities for adiabatic passage of a particle through a curve crossing in terms of the relative slopes of the diabatic (unperturbed) potentials and the Rabi frequency:

$$w = e^{-2\pi V^2/h\nu|F_1 - F_2|} \ , \tag{9}$$

where $F_{1,2}$ are the slopes $d\phi/dR$ of the diabatic curves (ϕ is the potential), and v is the velocity of internuclear motion at the crossing. The formula relates the probability of transfer to the similarity between the two states (how far they are from each other and how much the slopes differ) and to the time spent near the crossing, which varies inversely with v. The calculated probabilities of diabatic crossings (jumps between the states) for the vibrational levels above the classical dissociation threshold are shown in Table I.

Following the transition the ion dissociates into H^+ and a neutral hydrogen atom. This dissociation path is *path 1* in Fig. 13. The curves on this figure were calculated at parallel intensity $I_{\rm pl} = 3.5 \times 10^{13}$ W/cm^2. The kinetic energy of the detected proton must satisfy

$$E_{\rm path\,1} = (E_n + \hbar\omega - E_D)/2 \ , \tag{10}$$

where E_n is the potential energy of the H_2^+ ion in the nth vibrational level and E_D is the final potential energy of the system. The division by 2 shows that the available energy is divided equally between the two fragments.[16] Final proton energies for unperturbed vibrational levels of H_2^+ are marked on the bottom of Fig. 4.

The probability of a three-photon transition may be

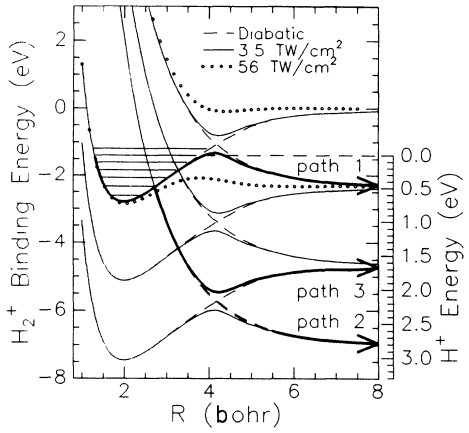

FIG. 13. Results of Floquet calculations for 532-nm light. Solid curves: adiabatic potential for $I_{\rm pl} = 3.5 \times 10^{13}$ W/cm^2; dashed curves: diabatic (unperturbed) $1s\sigma_g$ and $2p\sigma_u$ states shifted by $n\hbar\omega$.

calculated the same way. In this case, the transition occurs at a smaller internuclear separation where the three-photon resonance occurs, and each fragment has $\hbar\omega$ more energy:

$$E_{\rm path\,2} = (E_n + 3\hbar\omega - E_D)/2 = E_{\rm path\,1} + \hbar\omega \ . \tag{11}$$

The path is marked as *path 2* in Fig. 13. Probabilities for three-photon transitions are given in Table I.

Yet a third possibility exists, shown as *path* 3 in Fig. 13. This is three-photon excitation of the $1s\sigma_g$ state, followed by an adiabatic transition back onto the bound potential curve. This corresponds to three-photon absorption at the three-photon resonance, followed by one-photon stimulated emission at the one-photon resonance. The outgoing fragment energies are midway between the other two, so that the three peaks are separated by $\hbar\omega/2$.

The appearance of multiple peaks in the fragment dissociation spectrum is analogous to the additional peaks in the electron spectra in above-threshold ionization. Thus this new phenomenon has been called *above-threshold dissociation.*[9]

The Landau-Zener calculations clearly show that at

TABLE I. Probabilities.

(a) One-photon diabatic crossing probability, 532 nm

Intensity	$v''=4$	$v''=5$	$v''=6$	$v''=7$
3.5×10^{12} W/cm^2			0.04	0.18
7×10^{12} W/cm^2			0.007	0.03
1.4×10^{13} W/cm^2		5×10^{-5}	0.001	0.005
3.2×10^{13} W/cm^2	3×10^{-10}	4×10^{-7}	5×10^{-6}	2×10^{-5}

(b) Three-photon adiabatic noncrossing probability, 532 nm

Intensity	$v''=2$	$v''=3$	$v''=4$	$v''=5$	$v''=6$	$v''=7$	Multiplier
3.5×10^{12} W/cm^2	5.01	3.49	2.85	2.51	2.28	1.97	$\times10^{-7}$
7×10^{12} W/cm^2	2.27	1.57	1.29	1.14	1.04	0.893	$\times10^{-6}$
1.4×10^{13} W/cm^2	2.53	1.75	1.44	1.26	1.15	0.993	$\times10^{-5}$
3.2×10^{13} W/cm^2	2.37	1.64	1.35	1.19	1.08	0.932	$\times10^{-4}$
5.6×10^{13} W/cm^2	1.65	1.14	0.94	0.83	0.75	0.65	$\times10^{-3}$

our intensities, one-photon transitions are greatly favored over three-photon transitions. Path 1 is most probable, followed by path 3 next, and path 2 last. Quantitative comparisons with experiments require averaging over the inhomogeneous intensity distribution in the laser focus. Since the distribution of the source ions in the focal region is not certain, the problem is compounded. However, the main conclusions are well supported by the experiment: most of the proton signal is in the low-energy peak, with less in the peak that is one-half photon higher in energy, and still less in the peak still one-half photon higher.

The specific mechanism of bond softening in H_2^+ proposed here is corroborated by observations of two additional intensity-dependent effects. As the light intensity increases, the local maximum in the adiabatic potential curve becomes lower, so that lower vibrational levels become unbound (see Fig. 12). This increases the relative number of low-energy protons and broadens the low-energy peak, as seen in Fig. 4.

The other intensity effect is observed in the angular distribution of protons. As the light intensity grows, so does its parallel component. Since the dissociation probability depends on parallel component of intensity only, the restriction on alignment with the field relaxes at higher intensity, leading to a broadening of the angular distribution with intensity (see Fig. 5).

Deformation of potential curves with intensity affects not only the proton spectra, but electron spectra as well. As the intensity grows, the bottom of the potential well becomes more shallow, so that vibrational eigenvalues decrease in energy. One should expect a corresponding increase in the energies of the outgoing photoelectrons (see Fig. 14), or at least an increase in the width of the electron peaks. The broadening that we see in the electron data at higher intensities may be evidence for this (see Fig. 2).

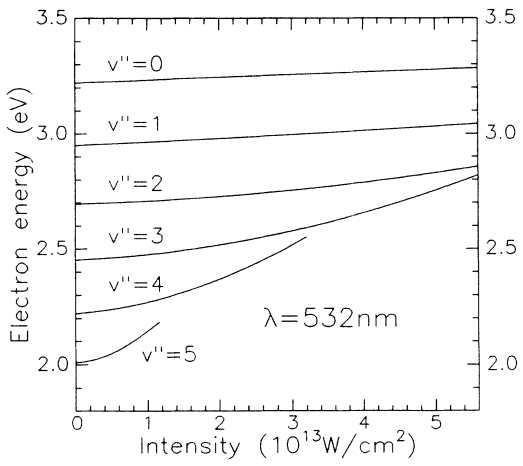

FIG. 14. As the parallel component of the light intensity grows, the vibrational eigenvalues of $2p\sigma_u$ state become lower, increasing the kinetic energy of the electrons emitted during photoionization. The figure shows the predicted energy of electrons emitted during eight-photon ionization of H_2 by 532-nm light into different vibrational levels v^+ of $1s\sigma_g$ state, as a function of I_{pl}.

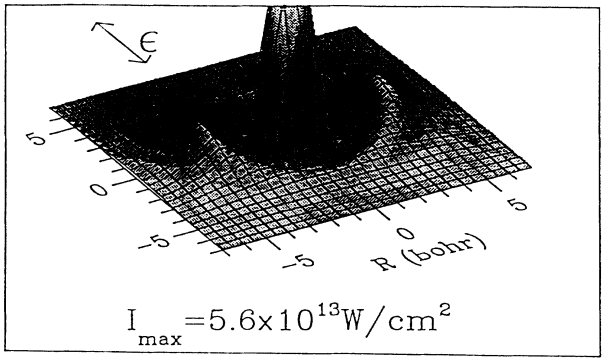

FIG. 15. Effective potential well formed by the adiabatic crossing of the $1s\sigma_g$ and $2p\sigma_u$ states as a function of the relative orientation of the internuclear axis and the laser polarization.

In addition, the electron spectrum is linked to any changes in Franck-Condon factors with intensity, so that the relative distribution could change in a predictable way. Unfortunately, we believe that two factors keep us from seeing this effect in the 532-nm experiment. First, the ionization rate is likely to be much less strongly dependent on the orientation of the internuclear axis than is the dissociation rate. Therefore most of the ATI occurs at rather small *parallel* intensities, even though they are large *total* intensities. Furthermore, as discussed in Sec. III A 1, our high-intensity spectra probably contain a significant number of electrons from ATI in atomic hydrogen, produced after dissociation of H_2^+. This ATI spectrum unfortunately lies on top of the H_2 ATI spectrum for 532 nm.

This lowering of the vibrational eigenvalue as the parallel intensity increases creates a torque on the molecule, which might tend to cause it to precess or even align with the laser polarization. We can imagine the molecule moving in a three-dimensional potential well, with sides that become quite low along the laser polarization axis (Fig. 15). Mittleman has analyzed the corresponding classical problem of a vibrating rotor in an angle-dependent potential, and finds that the molecular trajectory can become chaotic for potential deformations that are great enough.[17] This idea is not needed to explain the 532-nm data, but it may be more important for longer wavelengths (see below).

To summarize this section, we find that a new phenomenon leads to rapid dissociation of H_2^+ in a laser field. This is the softening of the molecular bond. The spectrum of the ion fragments, their angular distributions, and the electron spectra all show that this new mechanism is the dominant effect in laser fields above 10^{13} W/cm^2.

B. Explanation of uv proton data

Insight gleaned from the 532-nm data can be applied to the uv (355-nm) proton energy spectra as well. The three paths for dissociation seen for green light are altered here because of the higher photon energy. In particular, the

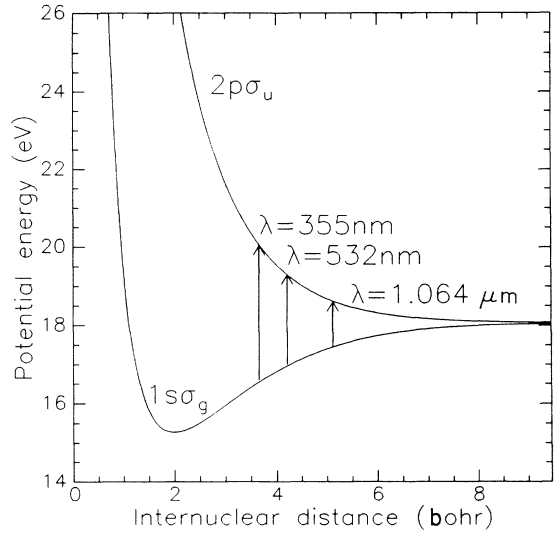

FIG. 16. One photon-resonance shifts to shorter internuclear distance for shorter wavelengths.

one-photon resonance occurs at smaller internuclear separation (see Fig. 16), so that the fragments are more energetic. In addition, the reduced bond length means that lower vibrational levels are unbound in weak fields. Combined with the fact that ions tend to populate the lower vibrational levels at this wavelength (see Fig. 6), this tends to lower the proton energies. Table II gives the Landau-Zener probabilities for one-photon transitions for the uv light. Because of the lower intensities used in the experiments, the three-photon crossing is much less probable at 355-nm light than at 532 nm, and in fact only one peak, corresponding to dissociation path 1, is observed.

The very low proton count rate in experiments involving 355-nm light explains why there are relatively few electrons due to the ionization of atomic hydrogen in the electron spectra. The relatively small rate for dissociation also argues against the decay mechanism proposed by Verschuur, Noordam, and van Linden van den Heuvell and described above, involving excitation to dissociating doubly excited states.

VI. ir DATA DISCUSSION

A. Electrons

The ionization of H_2 by 1.064-μm radiation remains an intriguing puzzle. We do not have a clear explanation for the broad featureless electron spectra with the extreme high-energy tails. However, there are some interesting clues. The fastest electrons seem to appear with kinetic energies close to the peak value of ponderomotive potential in the laser focus. An early suggestion was that the electrons simply pick up their kinetic energies from the ponderomotive scattering as they leave the light focus.[18] However, we were able to rule out this idea by measuring the angle dependence of the detected electrons in the azimuthal plane. If all of the electrons' energy did come from the ponderomotive scattering, the angular distribution should have become more isotropic in the higher-energy parts of the spectrum, since a larger fraction of these electrons' momentum is transferred to them by the axially symmetric laser focus.[2] However, the opposite is observed: the angular distributions in Fig. 9 show that electrons with higher kinetic energies tend to be more closely aligned with the direction of field polarization. This argues against simple ponderomotive scattering.

Another very interesting idea stems from the classical description of a hydrogen molecule as a vibrating rotor with a tensor polarizability.[17] Left free, the classical molecule vibrates and rotates. An external high-frequency ac electric field produces an aligning torque, so that the molecule takes on several different kinds of motion with different time scales, i.e., vibration precession, and nutation. A small torque causes the angular momentum vector of the molecule to precess around the laser polarization, as the nutation angle undergoes slow anharmonic oscillations. However, as the laser intensity grows, so does the induced polarization, the torque, and the nutation. An intensity-dependent parameter q^2 may be defined as follows:

$$q^2=\frac{\Delta\alpha E^2}{4MR^2\omega_R^2}\ , \tag{12}$$

where E is the magnitude of the applied electric field (proportional to the square root of the light intensity), M is hydrogen molecule's reduced mass, R the internuclear distance, $\Delta\alpha$ the difference between parallel and perpendicular polarizability of hydrogen molecule, and ω_R is the rotational frequency around the electric field. For $q^2>\frac{1}{2}$, which corresponds to a light intensity of 8×10^{13} W/cm^2, the motion of the vibrating rotor changes qualitatively. The nutation grows, forcing the molecule close to alignment. The critical intensity for this is surpassed by an order of magnitude in our ir experiments, so this mechanism may contribute to our results.

B. Protons

The proton energy spectrum is difficult to analyze without first understanding the electron spectrum.

TABLE II. One-photon diabatic crossing probability 355 nm.

Intensity	$v''=3$	$v''=4$	$v''=5$	$v''=6$	$v''=7$
3.5×10^{12} W/cm^2		0.161	0.36	0.449	0.504
7×10^{12} W/cm^2		0.07	0.163	0.224	0.269
1.4×10^{13} W/cm^2	7.4×10^{-5}	0.007	0.021	0.036	0.051
3.2×10^{13} W/cm^2	2×10^{-6}	4×10^{-5}	2×10^{-4}	5×10^{-4}	0.001

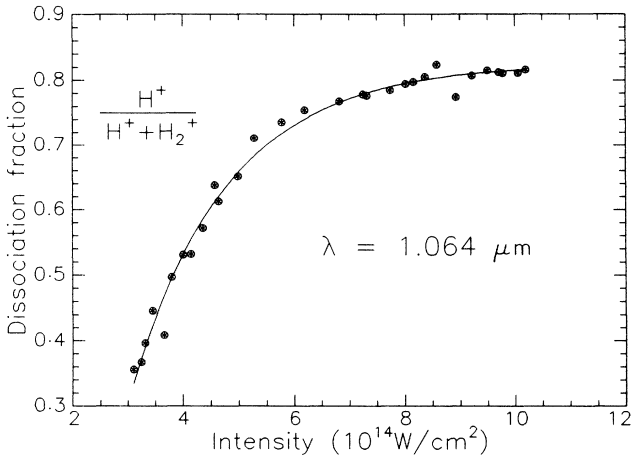

FIG. 17. Hydrogen dissociation fraction vs intensity for 1.064-μm light.

Nonetheless, several familiar features emerge in the proton data. The ion fragments have very low energies, which implies some kind of potential deformation similar to bond softening. Also, there is some structure in the spectrum, although not as distinct as for 532 nm. Unlike data at the other laser wavelengths, the ir electron energy spectra do not supply clear information about ion populations in the different vibrational levels of the H_2^+ ground state. We know that H_2^+ was formed from charge-mass data (see Fig. 17), but we do not know how it was formed in detail.

If the normal bond-softening mechanism still holds for the 1.064-μm data, we should observe two more peaks corresponding to path 2 and path 3 in Fig. 13. The peak separations will be much smaller, however, only 0.58 eV. Given the large width of the peaks, these features of above-threshold dissociation may not be visible. In fact, we only observe a shoulder on the high-energy side of the distribution.

VII. CONCLUSION

In conclusion, we have discovered a number of new high-field phenomena in our observations of H_2 illuminated by intense infrared, visible, and ultraviolet light: (i) above-threshold ionization to various vibrational states in the molecular ion, (ii) high-energy electrons in ATI spectra at 1.064 μm, (iii) enhanced dissociation via the mechanism of bond softening, (iv) above-threshold dissociation, (v) evidence for alignment for the molecule in a high-intensity laser field. In future work, it would be particularly interesting to extend these studies to the regime of sub-picosecond pulses, where we might expect to identify specific ionization and dissociation pathways, and observe the dynamics of molecular alignment leading to above-threshold dissociation.

ACKNOWLEDGMENTS

We are thankful to many people, who via numerous discussions have helped us to shape our understanding of the collected data. Particularly useful were discussions with M. Mittleman, F. Mies, A. Giusti, and B. van Linden van den Heuvell and his students. We also are grateful to various members of the FOM–Institute for Atomic and Molecular Physics for providing advice and software for calculations of wave functions and Franck-Condon factors, and to the FOM–Institute for permitting this collaboration to take place through the extended visit of one of us (H.G.M.). H.G.M. received support for this work from the Nederlandse Organisatie voor Wetenschappelijk Ondezoek (NWO).

*Also at Department of Applied Physics, Columbia University, New York, NY.

†Permanent address: FOM–Institute for Atomic and Molecular Physics, Kruislaan 407, 1098 SJ Amsterdam, The Netherlands.

[1]P. Agostini, F. Fabre, G. Mainfray, G. Petite, and N. Rahman, Phys. Rev. Lett. **42**, 1127 (1979); P. Kruit, J. Kimman and M. Van der Wiel, J. Phys. B **14**, L597 (1981); S. I. Chu and J. Cooper, Phys. Rev. A **32**, 2769 (1985); M. Edwards, L. Pan, and L. Armstrong, Jr., J. Phys. B **18**, 1927 (1985); Z. Deng and J. H. Eberly, Opt. Soc. Am. B **2**, 486 (1985); A. Guisti-Suzor and P. Zoller, Phys. Rev. A **36**, 5178 (1987).

[2]R. R. Freeman, T. J. McIlrath, P. H. Bucksbaum, and M. Bashkansky, Phys. Rev. Lett. **57**, 3156 (1986).

[3]T. J. McIlrath, P. H. Bucksbaum, R. R. Freeman, and M. Bashkansky, Phys. Rev. A **35**, 4611 (1987).

[4]See, for example, P. H. Bucksbaum, in *Atomic and Molecular Processes with Short Intense Laser Pulses,* edited by A. D. Bandrauk (Plenum, New York, 1988), p. 149.

[5]C. Cornaggia, D. Normand, J. Morellec, G. Mainfray, and C. Manus, Phys. Rev. A **34**, 207 (1986); L. Bigio and E. R. Grant, J. Chem. Phys. **83**, 5361 (1985); L. Bigio, G. S. Ezra, and E. R. Grant, *ibid.* **83**, 5369 (1985); A. D. Bandrauk, and M. L. Sink, *ibid.* **74**, 1110 (1981); S.-I. Chu, *ibid.* **75**, 2215 (1981); S. L. Anderson, G. D. Kubiak, and R. N. Zare, Chem. Phys. Lett. **105**, 22 (1984); S. T. Pratt, P. M. Dehmer, and J. L. Dehmer, *ibid.* **105**, 28 (1984).

[6]M. H. Nayfeh, J. Mazumder, D. Humm, T. Sherlock, and K. Ng, in Ref. 4, p. 177.

[7]T. S. Luk and C. K. Rhodes, Phys. Rev. A **38**, 6180 (1988).

[8]J. W. J. Verschuur, L. D. Noordam, and H. B. van Linden van den Heuvell, Phys. Rev. A **40**, 4383 (1989).

[9]A. Guisti-Suzor, X. He, O. Atabek, and F. H. Mies, Phys. Rev. Lett. **64**, 515 (1990).

[10]T. E. Sharp, At. Data **2**, 119 (1971).

[11]The peak positions for 355-nm Xe photoelectron spectra are easily calculable. See, for example, D. Feldmann, D. Petring, G. Otto, and K. H. Welge, Z. Phys. D **6**, 35 (1987). We have collected spectra (unpublished) agreeing with the theoretical predictions for Xe.

[12]See, for example, R. R. Freeman, P. H. Bucksbaum, H. Milchberg, S. Darack, D. Schumacher, and M. E. Geusic, Phys. Rev. Lett. **59**, 1092 (1987).

[13]See, for example, G. Herzberg, *Molecular Spectra and Molecu-*

lar Structure I. Spectra of Diatomic Molecules (Van Nostrand Reinhold, New York, 1950).

[14]See, for example, F. H. M. Faisal, *Theory of Multiphonon Processes* (Plenum, New York, 1987).

[15]See, for example, L. D. Landau and E. M. Lifshitz, *Quantum Mechanics, Course of Theoretical Physics 3* (Pergamon, New York, 1965).

[16]According to momentum conservation, the energy is divided *almost* equally between the proton and the H atom. In reality, the energy difference is about 0.05%, which is far below the resolution of our spectrometer.

[17]M. Mittleman (private communication).

[18]A. Szoke (private communication).

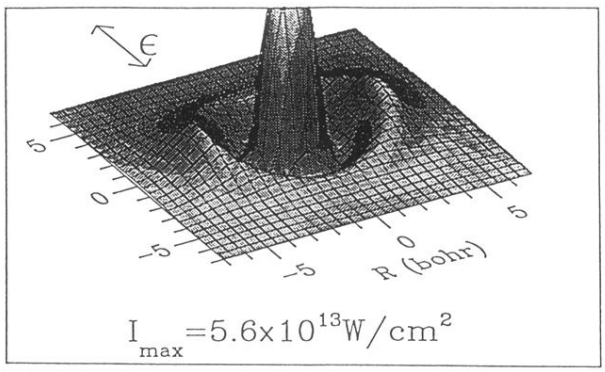

FIG. 15. Effective potential well formed by the adiabatic crossing of the $1s\sigma_g$ and $2p\sigma_u$ states as a function of the relative orientation of the internuclear axis and the laser polarization.